Antipodal-Vivaldi Meander-Line Antenna for 5G Applications

Jayendra Kumar[1] and Narayana Rao Palepu Researcher[2]

***Abstract*— A novel fifth-generation (5G) antenna design featuring a single element has been proposed to enhance antenna performance of bandwidth, cross-polarization, and gain parameters. This advanced antenna design incorporates a meander-line radiator and a defective ground plane (DGS) as its core structure. Several techniques have been employed to improve its capabilities. Adding neutralization lines to the antenna radiator enhanced the bandwidth. Additionally, the cross-polarization is reduced, and the antenna gain is enhanced by using an antipodal-vivaldi DGS (AVDGS). These design elements work together to improve the overall performance of the antenna. The suggested single-element antenna possesses a multi-wavelength structure with dimensions of $W \times L \times H = 28 \times 7 \times 1.6\ mm^3$, making it suitable for millimeter-wave applications. The antenna operates at a central frequency of 28 GHz and exhibits a -10 dB fractional bandwidth of 12.78%, a gain of 7 dBi, and a cross-polarization isolation of 17 dB in the E and H planes with the main lobe of the antenna positioned at $\pm 30°$.**

***Keywords*— 5G FR-II band, Antipodal antenna, Directional antenna, gain, Low profile antenna, Meander line antenna.**

I. INTRODUCTION

The evolution and advancements of cellular networks, specifically focusing on the transition from 2G/3G/4G to the upcoming 5G technology[1]. Implementing millimeter waves (mm Waves) in 5G networks, with frequencies between 30 and 300 GHz, allows for more efficient utilization of the mm-Wave spectrum, resulting in expanded coverage and significantly increased speeds[2]. Initially, the allocation of frequency bands for cellular systems by the Federal Communications Commission (FCC) is between 1 and 3 GHz, while modern cellular systems operate in the range of 7 to 21 GHz. Recently, the 5G spectrum has been allocated to the 28 GHz, 38 GHz, and 60 GHz bands, capable of penetrating buildings and crucial for indoor coverage and future cellular systems[3]. Increasing their size is unnecessary to improve the broadband performance of patch antennas. Instead, dispersed elements like inductive meander lines and slits can be utilized to reduce antenna resonance frequencies[4]. The Meander Line Antenna (MLA) is a concept that enables the miniaturization of 5G antenna arrays with high gain, low profile, beam phase shifting, and compact size compared to conventional microstrip antennas[5]. Cross polarisation is a significant issue with microstrip patch antennas (MPA) due to the substrate's high dielectric constant[6]. However, there are methods to reduce cross-polarisation without increasing the antenna's size and cost. One approach is considering the antenna's quality factor, or Q, while designing a compact and wideband antenna[7]. Innovative technologies, such as the MIMO[8], band notch[9], reconfigurable antenna[10], fractals[11], super substrates[12], meta-meterials[13] and neutralization lines (NL) [14] have been proposed to reduce antenna size and increase bandwidth. Another antenna technology, Antenna Vivaldi Antenna (AVA)[15] has surpassed standard patch of Antipodal Tapered Slot Antenna (ATSA)[16] technologies regarding gain, bandwidth, signal-to-noise ratio (S/N), response time, isolation, and cross-polarization. The AVA enables smaller, lighter, and more user-friendly mobile and wearable devices. Defective Ground Structure (DGS)[17] technology is utilized in microstrip patch filter antennas to lower their resonance frequency and improve reduction in cross-polarization. This technology involves incorporating slots or gaps in the ground plane of the antennas. DGS has garnered attention for its diverse benefits beyond its filter use.

The development of efficient and portable handheld devices capable of handling high bit rates at weak signal levels is a crucial focus in designing meandering 5G Frequency range-2 antennas. Other antenna enhancement techniques are employed to meander the radiator, such as embedding Quarter wave transformer feed, NL, AVA, and DGS to achieve broader bandwidth and gain. This approach efficiently covers the 5G mm Waves and reduces the antenna size without compromising its parameter performance. Section II provides meander radiator design parameters. Section III discusses the proposed Single Element(SE) antenna layout evolution mechanism, and in Section IV, single-element results are discussed further detail. Section V comes to a close with a formal conclusion.

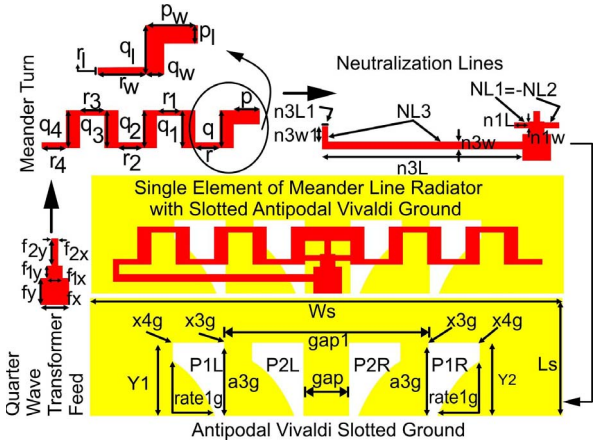

Fig. 1: Proposed Single Element Patch

II. ANTENNA DESIGN MECHANISM

The predominant losses of implementing MPA [18] with the full ground are caused by surface wave agitation, which

[1]J.Kumar is with Faculty of the School of Electronics, VIT-AP University, Amaravathi, Andhra Pradesh-522237, India jayendra854330@gmail.com

[2]N. R. Palepu Researcher is withthe School of Electronics, VIT-AP University, Amaravathi, Andhra Pradesh-522237, India pnarayana.usharama@gmail.com

causes a deterioration in bandwidth. Furthermore, waves on the surface can take in all the power that can be radiated to a spatial wavelength. The MLA conducting metal is periodically bent in a design to lower the resonant length and suppress the surface wave agitation . The meander line patch design formulas (1) to (8) for selecting an appropriate operating frequency from the empirical meander line formulas[19] and nomographs design formulas[20] followed by a description of the design parameters used to select the appropriate length (L) and width (W) of meander design parameters section.

Height of meander

$$S = 0.102\lambda_g \tag{1}$$

Distance of meander

$$d = 0.046\lambda_g \tag{2}$$

Width of meander

$$w = 0.013\lambda_g \tag{3}$$

Total length of antenna

$$NXS = \lambda_0/10 \tag{4}$$

N = number of turns, S = spacing between two meander lines.

Characteristic impedance of each meander section

$$Z_o = 276log\left(\frac{2S}{d}\right) \tag{5}$$

d = monopole wire diameter

Guided wavelength

$$\lambda_g = \frac{\lambda_0}{\sqrt{\varepsilon_{eff}}} \tag{6}$$

Free space wavelength

$$\lambda_0 = \frac{c}{f} \tag{7}$$

Effective permittivity:

$$\varepsilon_{eff} = \frac{\varepsilon_r + 1}{2} + \frac{\varepsilon_r - 1}{2}\left[\frac{1}{\sqrt{1 + \frac{10h}{w}}}\right] \tag{8}$$

Where,
h =height of substate
w =width of meander
ϵ_r = dielectric constant of given material
ϵ_{eff} = effective dielectric constant

III. DESIGN OF SINGLE ELEMENT

The proposed monopole meander line single antenna element is implemented using a dense meander antenna and opted for a compressed with $\lambda/4$ size. The antenna is made of a 1.6mm thick RT Duroid (RTD) substrate with a dielectric constant of ϵr=2.2 and a loss tangent of $\tan\delta$ = 0.0001. The detailed geometry of the single element evolution design is shown in Fig.1. Table I summarizes the proposed single-element optimized design parameter values in guided wavelength. Overall, the progression of the proposed antenna evolution is carried out in two distinct modules. The first module focuses on patch evolution, while the second addresses how the ground evolves. The patch evolution module starts at dual armed meander radiator (DAMR) ends at neutralization Line 3 (NL3), whereas at ground module is divided into two sections, the first of which begins at the single dumbelled DGS (Defective Ground Structure) and ends at the DDGS complementary Antipodal Vivaldi DGS (AVDGS) and the second at the AVDGS type-1 and ends at the AVDGS type-4 as shown in Fig.2. The volume of the antenna element, including the ground, is $28 \times 7 \times 1.6mm^3$. The neutralized line (NL) feeding unit is electrically coupled to a symmetric horizontal DAMR unit to expand bandwidth at high resonant frequency bands. The Meander Line Antenna (MLA), or folded unit, shortens the aerial length along the Y-axis, maintains similarity in E-field and H-field patterns, and reveals MLA impedance. The NL feeding contact area is strengthened to supply the requisite mutual inductance produced between the feed contact and the DAMR unit. An NL is made up of three rectangle branches, neutralization line1 (NL1), neutralization line2 (NL2), and neutralization line3 (NL3), with full ground deployed that are associated with the top RTD surfaces where $NL1 = -NL2$ and triggering is provided using a 50 microstrip QWT stepped center feed line. The NL offers a high-frequency resonance to improve the antenna's bandwidth and conducts electromagnetic impulses across antenna sections to prevent mutual coupling. On the lower side of the substrate, the DGS methods are embedded to undergo the improvement in cross-polarization. The properties of DGS have cross-polarization sharp decline, and slot etched over the ground plane modifies complex conjugate of capacitance and inductance to match the impedance, thus enhancing the possibilities of gain and bandwidth. Such an approach is added to meandered line neutralization design radiator with different slotted DGS methods. The DGS methods include the single dumbelled DGS (DDGS), DGS Array, AVDGS, DDGS complementary AVDGS, and AVDGS Type-1 to AVDGS Type-4.

TABLE I: Single element design optimised Parameter values

parameter	Value (mm)	parameter	Value (mm)	parameter	Value (mm)
Ws	28	pw	λ_g/5.4	n3L1	λ_g/10
Ls	7	ql	λ_g/3.2	n3W1	λ_g/20
fx	1.59	qw	λ_g/8.6	rate1g	550
f1x	0.75	rl	λ_g/5.4	gap	- λ_g/0.95
f2x	0.78	rw	λ_g/5.0	gap1	- λ_g/2.49
fy	1.6944	n1L	λ_g/21	a3g	λ_g/2.88
f1y	0.92	n1W	λ_g/5.4	a4g	λ_g/4.12
f2y	0.39	n3L	λ_g/15	x3g	λ_g/4.66
pl	λ_g/8.6	n3W	λ_g/0.6	x4g	- λ_g/4.81

IV. RESULTS AND DISCUSSION

Fig.3 illustrates the individual variation results of the top substrate patch DAMR neutralization lines, while Fig.4 depicts the parameters affecting the bottom substrate of AVDGS. Fig.3(a) presents the impact of the DAMR patch with the NL3 structure, showcasing improved gain and scattering parameters versus frequency. It also explores the

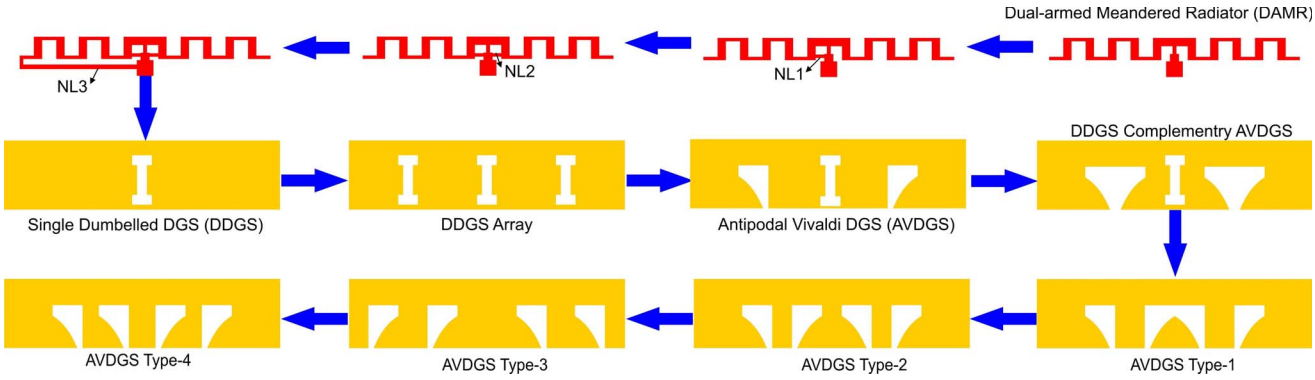

Fig. 2: Evolution of the proposed antenna.

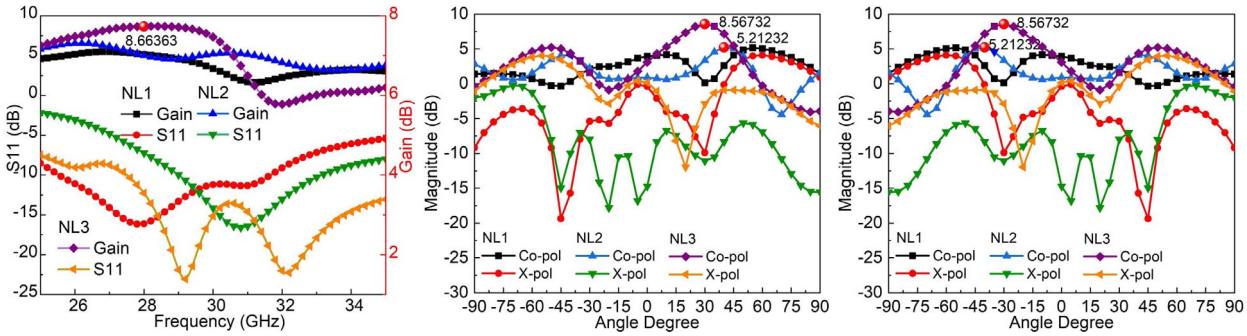

(a) (b) (c)

Fig. 3: Effect of neutralization line on antenna characteristics (a) Frequency versus S11 and antenna gain (b) E-plane co and cross polarization radiation (c) H-plane co and cross polarization radiation

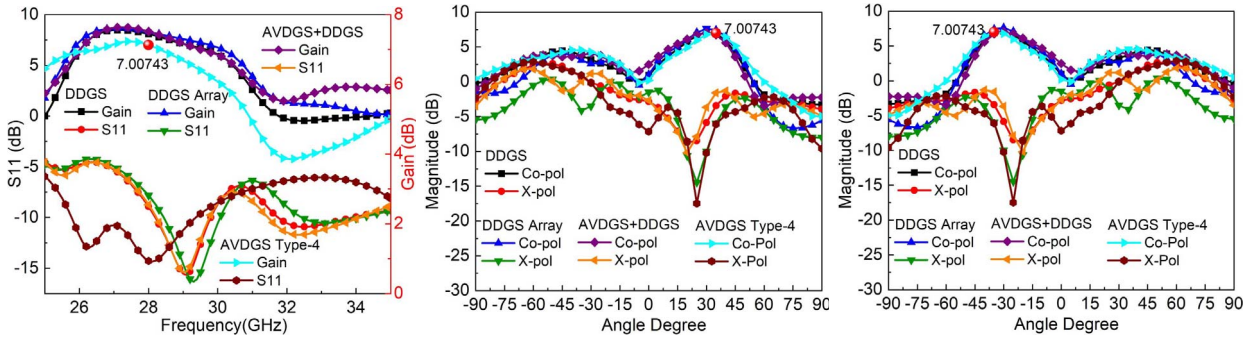

(a) (b) (c)

Fig. 4: Antenna characteristics against different DGS (a) Frequency versus S11 and antenna gain (b) E-plane co and cross polarization radiation (c) H-plane co and cross polarization radiation

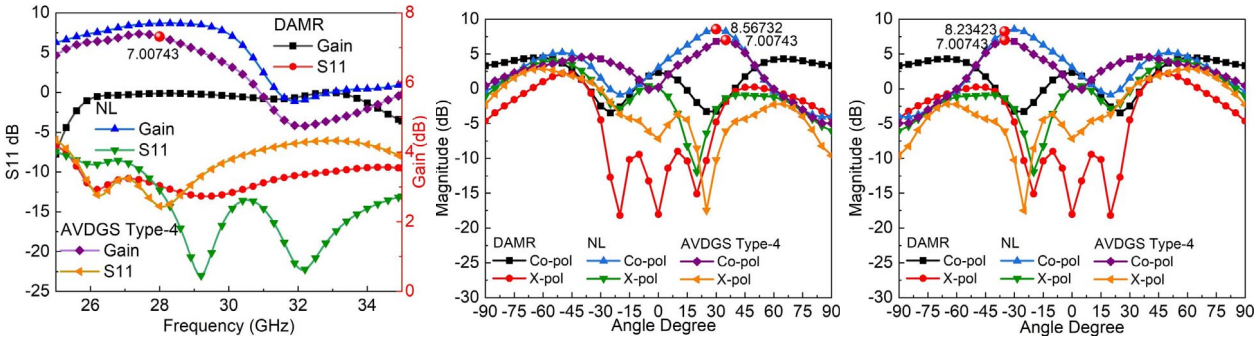

(a) (b) (c)

Fig. 5: Antenna characteristics in different evolution iterations (a) Frequency versus S11 and antenna gain (b) E-plane co and cross polarization radiation (c) H-plane co and cross polarization radiation

co-polarization (Co-Pol) and cross-polarization (X-Pol) of the E-Field Fig.3(b) and H-field Fig.3(c). The performance of NL1 and NL2 is limited to a single resonant frequency band, with more cross-polarization and gains of 5.1dBi and 5.2dBi, respectively. In contrast, NL3 demonstrates dual-band characteristics, an 8.6dBi gain, and a decrease in X-Pol from 8.6029 to -3.2778 observed at 29GHz. Fig.4(a) showcasing the gain and reflection coefficient responses of DDGS, DGS Array, DDGS complementary AVDGS, and AVDGS Type-4. Fig.4(b) and Fig.4(c) illustrate the 2D radiation patterns of the E-Field and H-field, respectively. The DDGS exhibits dual-band findings, a gain of 7.2dBi, and a decrease in X-Pol from 7.1605 to -5.8815 is observed at 32GHz. The DGS Array resonates at 29GHz with a gain of 7.6dBi, while its X-Pol drops from 7.6276 to -9.9852. Similarly, DDGS complementary AVDGS shows results in a single band at 29GHz, with a gain of 5.7dBi and a decrease in X-Pol from 5.7360 to 4.7076. Finally, AVDGS Type-4 exhibits a single-band resonance at 28GHz (25.78GHz - 29.36GHz), represented by a red sphere with a gain of 7.0dBi, while X-Pol drops from 7.0074 to -6.0792. Fig.5(a) compares DAMR, NL, and AVDGS-Type4. DAMR exhibits a moderate reflection coefficient but lags with zero gain, while AVDGS Type-4 satisfies the n261 spectrum frequency and demonstrates excellent S11 gain versus frequency. Fig.5(b) depicts AVDGS Type-4 E-Field and H-field co-polarization and cross-polarization in Fig.5(c).

V. CONCLUSION

A single-element RT duroid antenna measuring $28mm \times 7mm \times 1.6mm$ is proposed and simulated in HFSS 2021R1. The simulated results reports since inserting the QWT feed and NL rectangle structures between the two meander-line antenna units, the mutual coupling has significantly been reduced, the impedance matching has been enhanced, and the fractional bandwidth has increased to 12.78 %. This configuration of three rectangular neutralization lines acted as a waveguider. An MLA microstrip antenna on top and four defective ground vivaldi structures on the substrate's underside can reduce cross-polarization by 17 dB, while also generating 7 dBi in gain. The results show that the single-element design is optimal for 5G millimeter-wave operations in the n261 frequency range.

REFERENCES

[1] Ravi, Kiran Chand, and Jayendra Kumar. "Multi-directional Wideband Unit-element MIMO Antenna for FR-2 Band 5G Array Applications," *Iranian Journal of Science and Technology, Transactions of Electrical Engineering*, 46.2 (2022): 311-317.

[2] Ravi, Kiran Chand, and Jayendra Kumar. "Miniaturized Parasitic Loaded High-Isolation MIMO Antenna for 5G Applications," *Sensors*, 22.19 (2022): 7283.

[3] Jang, Tae Hwan, et al. "60 GHz low-profile, wideband dual-polarized U-slot coupled patch antenna with high isolation," *IEEE Transactions on Antennas and Propagation*, 67.7 (2019): 4453-4462.

[4] Palepu, Narayana Rao, and Jayendra Kumar. "Neutralized meander line patch antipodal vivaldi defected ground millimeter-wave antenna array," *AEU-International Journal of Electronics and Communications*, (2023): 154663.

[5] Acharya, Puja, et al. "Miniaturized omnidirectional satellite phone antenna inspired by meander line radiator and metamaterial integrated ground plane," *International Journal of Information Technology*, 14.6 (2022): 2981-2990.

[6] Zheng, Dongze, Yue-Long Lyu, and Ke Wu. "Longitudinally slotted SIW leaky-wave antenna for low cross-polarization millimeter-wave applications," *IEEE Transactions on Antennas and Propagation*, 68.2 (2019): 656-664.

[7] Swetha, Avula, and Kurukundu Rama Naidu. "Miniaturized antenna using DGS and meander structure for dual-band application," *Microwave and Optical Technology Letters*, 62.11 (2020): 3556-3563.

[8] BharathiDevi, Boyapati, and Jayendra Kumar. "Small frequency range discrete bandwidth tunable multiband MIMO antenna for radio/LTE/ISM-2.4 GHz band applications," *AEU-International Journal of Electronics and Communications*, 144 (2022): 154060.

[9] Bharathidevi, Boyapati, Jayendra Kumar, and Narayana Rao Palepu. "Band Rejection in Wideband Partial Ground Plane Antennas Using Defected Ground Structure," *Advances in Communication, Devices and Networking: Proceedings of ICCDN 2021. Singapore: Springer Nature Singapore*, 2022. 309-317.

[10] Nikam, Pritam B., et al. "Low-profile bandwidth and E-plane radiation pattern reconfigurable patch antenna for sub-6 GHz 5G applications," *AEU-International Journal of Electronics and Communications*, 157 (2022): 154415.

[11] Sharma, Narinder, and Sumeet Singh Bhatia. "Comparative analysis of hybrid fractal antennas: A review," *International Journal of RF and Microwave Computer-Aided Engineering*, 31.9 (2021): e22762.

[12] Dey, Shuvashis, Md Shamsul Arefin, and Nemai Chandra Karmakar. "Design and experimental analysis of a novel compact and flexible super wide band antenna for 5G," *IEEE Access*, 9 (2021): 46698-46708.

[13] Alibakhshikenari, Mohammad, et al. "Impedance bandwidth improvement of a planar antenna based on metamaterial-inspired T-matching network," *IEEE Access*, 9 (2021): 67916-67927.

[14] Kumar, Praveen, Tanweer Ali, and Manohara Pai Mm. "Characteristic mode analysis-based compact dual band-notched UWB MIMO antenna loaded with neutralization line," *Micromachines*, 13.10 (2022): 1599.

[15] J. -Y. Deng, R. Cao, D. Sun, Y. Zhang and L. -X. Guo,"Bandwidth Enhancement of an Antipodal Vivaldi Antenna Facilitated by Double-Ridged Substrate-Integrated Waveguide," *IEEE Trans. Antennas Propag.*, vol. 68, no. 12, pp. 8192-8196, Dec. 2020.

[16] Li, Jinlun, et al. "Ultrawideband antipodal tapered slot antenna with reflectionless notched band," *IEEE Antennas and Wireless Propagation Letters*, 21.3 (2021): 431-435.

[17] Malhotra, Rahul, Srishti Sharma, and Rajiv Nehra. "Miniaturized Patch Antenna That Uses Corner Triangles with Cloud Shape DGS," *2021 IEEE Mysore Sub Section International Conference (MysuruCon)*, IEEE, 2021.

[18] D. Mathur, S. K. Bhatnagar and V. Sahula, "Quick Estimation of Rectangular Patch Antenna Dimensions Based on Equivalent Design Concept," *IEEE Antennas Wireless Propag. Lett.*, vol. 13, pp. 1469-1472, 2014.

[19] Shoaib, Muhammad Muneeb, and Shafayat Abrar. "Planar Inverted-F Antenna for Portable Devices: An Empirical Study of the Resonant Frequency and Fractional Bandwidth," *2020 13th International Conference on Communications (COMM)*, IEEE, 2020.

[20] M. A. Ullah, R. Keshavarz, M. Abolhasan, J. Lipman, K. P. Esselle and N. Shariati, "A Review on Antenna Technologies for Ambient RF Energy Harvesting and Wireless Power Transfer: Designs, Challenges and Applications," *IEEE Access*, vol. 10, pp. 17231-17267, 2022.